J Electr Eng Technol.2018; 13(1): 315-325
http://doi.org/10.5370/JEET.2018.13.1.315

ISSN(Print) 1975-0102
ISSN(Online) 2093-7423

Optimum Air-Gap Flux Distribution with Third Harmonic Rotor Flux Orientation Adjustment for Five-Phase Induction Motor

Min Kang*, Wenjuan Yu, Zhengyu Wang***, Wubin Kong† and Ye Xiao*****

Abstract – This paper investigates optimum air-gap flux distribution with third harmonic rotor flux orientation adjustment for five-phase induction motor. The technique of objective is to generate a nearly rectangular air-gap flux, and it improves iron utilization under variation loading conditions. The proportional relations between third harmonic and fundamental plane currents is usually adopted in the conventional method. However, misalignment between fundamental and third harmonic component occurs with variation loading. The iron of stator teeth is saturated due to this misalignment. This problem is solved by third harmonic rotor flux orientation adjustment simultaneously, and direction and amplitude are changed with mechanical load variation. The proposed method ensures that the air-gap flux density is near rectangular for a maximum value from no load to rated load. It is confirmed that the proposed method guarantees complete both planes decoupling with third harmonic flux orientation adjustment. The effectiveness of the proposed technique is validated experimentally.

Keywords: Air-gap flux, Five-phase induction motor, Third harmonic, Nearly rectangular, Orientation adjustment

1. Introduction

In recent years, high power motor drives are required in some applications, such as locomotive traction, electric ship propulsion and aircraft drives. Multiphase motor drives are suitable for higher power condition with more extra phase, and the current per phase is reduced for a given phase voltage and total power rating [1-3]. Moreover, high performance multiphase induction motor (IM) drives have other advantages, such as reliability, robustness and high torque density [4-6].

In multiphase drives, the fundamental and harmonic planes can be controlled independently, and this property allows reducing the torque pulsation. The reliability is a distinguished merit compared to three-phase drive, and fault-tolerant control strategies for continuous smooth and steady operation without motor halt [7-9]. The global fault-tolerant control technique is flexibility and simplicity in dealing with all possible fault conditions [10].

High torque density multiphase motor drive to improve the delivered torque has been of interest to researchers [11-12]. The enhancement benefits from the harmonic air-gap fluxes, which effectively increase the magnitude of fundamental flux density without iron saturation [13-14]. DC-link voltage utilization is also improved by modulation strategies for the pulse width modulation with harmonic current injection [15-18]. The motor drive is fed by quasi-rectangular voltage, and the flatted air-gap flux density waveform is obtained. The quasi-trapezoidal air-gap flux density is essential for torque density improvement [19-20].

Some more studies have investigated the performance of optimum air-gap flux distribution more deeply [21-24]. A novel control method for a six-phase IM with nearly square air-gap flux density is proposed with no vector transformation, because the stator phase windings act as either or torque-producing phases [25]. The study in [26] presents steady-state analysis and performance of an eleven-phase IM when harmonic injection up to ninth harmonic. For the same RMS fundamental current, the motor could be overloaded by approximately 37.5%, and the corresponding increase in the RMS phase current is 25%. In [27], the use of genetic algorithm is proposed to determine the optimum quasi-square wave flux density distribution for an eleven-phase IM, and the paper indicates that the field harmonic contribution of order greater than five is negligible. The study in [28] reveals that the high-order spatial harmonics produce high loss in the stator back iron, and the stator back iron is increased by 20% with third harmonic injection.

The study in [29] extends the speed operation range, and the amplitude of the field harmonics is progressively reduced to ensure the widest possible operation at high speeds. However, little research has been presented on loaning variation effect on air-gap flux density distribution. An improved flux pattern is produced with a synchronization block, which is used to lock relative position

† Corresponding Author: State Key Laboratory of Advanced Electromagnetic Engineering and Technology, Huazhong University of Science and Technology, China. (wubinkong@126.com)
* College of Automation and Electrical Engineering, Zhejiang University of Science and Technology, China.
** Central China Branch of State Grid Corporation of China, China.
*** Hunan CRRC Times Electric Vehicle Co. LTD., China.
Received: June 16, 2017; Accepted: October 20, 2017

between fundamental and third harmonic fluxes [30]. The shortage of this method is that the gain in proportional loop should be limited to avoid system instability. A promoted controller gives a nearly flat flux pattern irrespective of mechanical loading, and it calculates the direct and quadrature current components of the third harmonic plane as a nonlinear function. However, this controller neglects that the third harmonic flux orientation is changed in time due to load variation, which is not synchronized with fundamental flux orientation. Moreover, the derivation of the electromagnetic torque calculation in the third harmonic plane is not correct. Concerning this problem, this paper improves the analysis in [31] to rotor flux angle adjustment between fundamental and third harmonic plane.

In this paper, the proposed method is investigated for optimum air-gap flux distribution with third harmonic rotor flux orientation adjustment for five-phase IM. The relations between rotor flux and air-gap flux are illustrated by vector diagram in both planes. The third harmonic rotor flux orientation acts as a real-time adjustment under mechanical load variation. Then, the direct and quadrature current components in the third harmonic are derived as a nonlinear function of the fundamental ones. The derived function ensures that the optimum air-gap flux density in various mechanical loads, and it makes corrections for electromagnetic torque calculation in [31] for the third harmonic plane. The performance of the proposed method is compared with the conventional controller that has a constant relation between the command current in both planes. Finally, a five-phase IM drive is constructed, and experimental results verify the feasibility of the proposed method.

2. Vector Control in the Dual-Planes

2.1 Five-phase IM model

The topology for five-phase IM drive is shown in Fig.1, and the typical isolated neutral is adopted. Five-phase inverter configuration is used to drive a star connected with squirrel-cage IM.

This paper adopts a four-pole five-phase induction motor with identical quasi-concentrated stator windings. The stator windings are distributed with 72° spatial angle

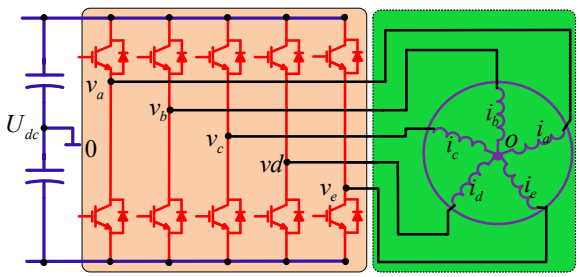

Fig. 1. Topology of five-phase IM drive

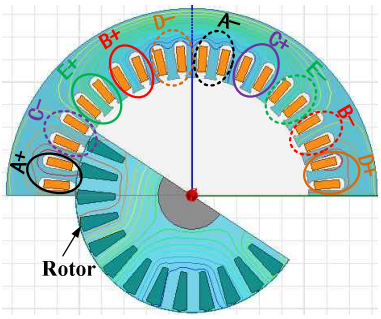

Fig. 2. Sketch of stator winding distribution

and each phase occur eight stator slots, as shown in Fig. 2. Each stator slot has 6 conductors and the squirrel cage rotor has 26 bars. The main dimensions and rated parameter for five-phase IM is contained in the Appendix.

By vector space decomposition, the fundamental and third harmonic of the motor are decoupled in the d_1-q_1 and d_3-q_3 synchronous reference frame. This model is similar to that in [30], and orthogonal matrix are used to transform stator quantities between the *a*-*b*-*c*-*d*-*e* natural reference frame and the d_1-q_1-d_3-q_3-*n* synchronous reference frame. The dual-plane vector control is set in the synchronous reference frame.

2.2 Dual-plane vector control

This section studies the dual-plane vector control with third harmonic injection, and indirect field orientation control (IFOC) is used for decoupled flux and torque control [20].

It is assumed that the fundamental and third harmonic rotor flux linkages are attached to d_1, d_3 axes, and no linkages on the q_1, q_3 axes in IFOC

$$\begin{cases} \psi_{rd1} = \psi_{r1} \\ \psi_{rd3} = \psi_{r3} \end{cases} \tag{1}$$

In IFOC, the direct current represents the magnetizing current, and the relationship between rotor fluxes and direct currents at steady state are

$$\begin{cases} i_{sd1} = \dfrac{\psi_{rd1}}{L_{m1}} \\ i_{sd3} = \dfrac{\psi_{rd3}}{L_{m3}} \end{cases} \tag{2}$$

To maintain a quasi-trapezoidal air-gap flux density distribution, the optimum air-gap flux density is described as

$$B_m(\phi_s) = B_{m1}(\sin\phi_s + k_3 \sin 3\phi_s) \tag{3}$$

where B_{m1} is amplitude for the fundamental component,

and ϕ_s is electrical angle. k_3 is gain for third harmonic flux density, and the value is 1/6 for the optimum air-gap flux density [20]. Substituting (3) into (2), the relationship between the direct components are

$$i_{sd3} = \frac{k_3}{3}\frac{L_{m1}}{L_{m3}} i_{sd1} \tag{4}$$

The relation between the quadrature components can be derived from the slip frequency

$$\begin{cases} \omega_{s1} = \dfrac{L_{m1}}{\tau_1 \psi_{r1}} i_{sq1} \\ \omega_{s3} = \dfrac{L_{m3}}{\tau_3 \psi_{r3}} i_{sq3} \end{cases} \tag{5}$$

where L_m is magnetizing inductance. Substituting (5) into $\omega_{s3} = 3\omega_{s1}$, the quadrature component relation between fundamental and third harmonic plane is

$$i_{sq3} = k_3 \frac{L_{m1}}{L_{m3}}\frac{\tau_3}{\tau_1} i_{sq1} = \frac{k_3}{k_{r3}}\frac{L_{m1}}{L_{m3}}\frac{L_{r3}}{L_{r1}} i_{sq1} \tag{6}$$

where $k_{r3} = R_{r3} / R_{r1}$, and it is represent the rotor resistance ratio between fundamental and third harmonic plane [31]. k_{r3} is unity if the skewing effects are neglected, and the Eq. (5) can be simplified

$$i_{sq3} = k_3 i_{sq1} \tag{7}$$

Substituting (2), (4) and (7) into torque expression in IFOC, the torque enhancement can be expressed as a function of the direct and quadrature current

$$\begin{cases} T_{e1} = \dfrac{5P}{4}\dfrac{L_{m1}}{L_{r1}} \psi_{r3} i_{sq1} \\ T_{e3} = \dfrac{15P}{4}\dfrac{L_{m3}}{L_{r3}} \psi_{r3} i_{sq3} = \dfrac{k_3^2}{k_{r3}} T_{e1} \end{cases} \tag{8}$$

The motor toque gain due to third harmonic injection is given

$$T_{Gain} = K(1 + \frac{k_3^2}{k_{r3}}) \tag{9}$$

where K is the increase in the fundamental flux due to harmonic injection [22], and the is equal to 1.155.

Torque/RMS is key characteristic for motor performance, and it is necessary to calculate the RMS phase current. The total direct axis current is

$$i_{sd} = K i_{sd1} \sqrt{1 + (\frac{k_3}{3}\frac{L_{m1}}{L_{m3}})^2} \tag{10}$$

Similarly, the total quadrature current is

$$i_{sq} = i_{sq1} \sqrt{1 + (\frac{k_3}{k_{r3}}\frac{L_{m1}}{L_{m3}}\frac{L_{r3}}{L_{r1}})^2} \tag{11}$$

Similarly, the total quadrature current is

$$I_s = \sqrt{i_{sd}^2 + i_{sq}^2} / \sqrt{2} \tag{12}$$

3. Optimum Air-Gap Flux Density Distribution with Proposed Method

3.1 Air-gap flux density distribution

The dual control for five-phase IM is based on IFOC, and the rotor flux orientations are aligned to $\vec{\psi}_{r1}$ and $\vec{\psi}_{r3}$. The air-gap flux density distribution is related to $\vec{\psi}_{m1}$ and $\vec{\psi}_{m3}$ directly [31], and the vectors relation between rotor flux and air-gap flux is shown in Fig. 3. The angle between rotor flux and air-gap flux depends on mechanical loading, since there is no guarantees that air-gap flux space phasor diagram for two planes are aligned.

The misalignment causes distortion of the flux density distribution, then the air-gap flux density expression in (3) should be modified

$$B_m(\phi_s) = B_{m1}(\sin\phi_s + k_3 \sin(3\phi_s - \delta_3)) \tag{13}$$

where δ_3 is misalignment angle between fundamental and third harmonic component.

The desired air-gap flux density distribution is depicted in Fig. 4(a), where both the fundamental and third components are aligned. Meanwhile, the value of δ_3 is equal to zero. The ideal distribution has two peaks at 60° and 120°. However, the waveform in Fig. 4(b) illustrates the same case with a 9° misalignment between two flux density components due to a certain mechanical loading. It is shown that the first peak at 60° is enlarged, and the second peak is minimized. Accordingly, it results in stator iron saturation. The traditional control method with constant gains neglects this effect, since it focuses on the

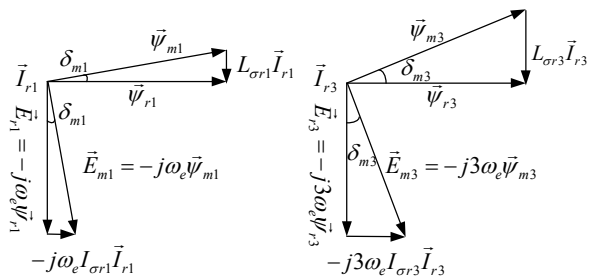

Fig. 3. Vectors relation between the rotor flux and air-gap flux

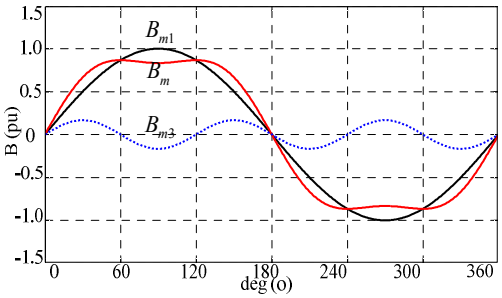

(a)

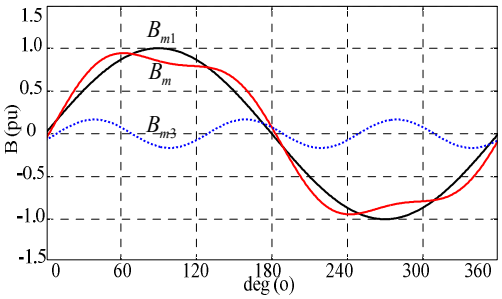

(b)

Fig. 4. Waveforms of flux density distribution

rotor flux linkage rather than air-gap flux linkage.

The air-gap flux orientation control is suitable for air-gap flux density optimization, but the control strategy is rather complicated without decoupling control. Hence, the promoted control in the dual-plane should be investigated. The vectors relation between rotor flux and air-gap flux is demonstrated in Fig. 3. δ_{m1} is the phase angle between rotor flux and air-gap flux for the fundamental plane, and δ_{m3} is the phase angle for the third harmonic plane. The expressions of δ_{m1} and δ_{m3} are

$$\begin{cases} \delta_{m1} = \sin^{-1}(\dfrac{L_{\sigma r1} i_{r1}}{\psi_{m1}}) \\ \delta_{m3} = \sin^{-1}(\dfrac{L_{\sigma r3} i_{r3}}{\psi_{m3}}) \end{cases} \tag{14}$$

The space phase of the air-gap flux (ψ_{m1} and ψ_{m3}) should be aligned to obtain a nearly rectangular flux distribution. The condition is achieved by

$$\delta_{m3} = 3\delta_{m1} \tag{15}$$

The derivation is included in [31] indicates that the direct and quadrature current components are calculated as a nonlinear function to satisfy the Eq. (15). However, the promoted controller in [31] has neglected that the third harmonic flux orientation is changed in time due to load variation, which is not synchronized with fundamental flux orientation. Concerning this problem, the proposed method with third harmonic rotor flux orientation adjustment is elaborated in section B.

3.2 The Proposed Method with Third Harmonic Rotor Flux Orientation Adjustment

The phase angle expression for fundamental and third harmonic plane in (14) should satisfy Eq. (15)

$$\sin^{-1}(\frac{L_{\sigma r3} i_{r3}}{\psi_{m3}}) = 3\sin^{-1}(\frac{L_{\sigma r1} i_{r1}}{\psi_{m1}}) \tag{16}$$

To obtain a near quasi-square air-gap flux distribution, the amplitude relation between ψ_{m1} and ψ_{m3} is

$$\psi_{m3} = \frac{k_3}{3}\psi_{m1} \tag{17}$$

where

$$\begin{cases} \psi_{m1} = \sqrt{\psi_{md1}^2 + \psi_{mq1}^2} \\ \psi_{m3} = \sqrt{\psi_{md3}^2 + \psi_{mq3}^2} \end{cases} \tag{18}$$

In IFOC control strategy, the quadrature current relation in the stator and rotor is

$$\begin{cases} i_{rq1} = \dfrac{L_{m1}}{L_{r1}} i_{sq1} \\ i_{rq3} = \dfrac{L_{m3}}{L_{r3}} i_{sq3} \end{cases} \tag{19}$$

Substituting (17) and (19) into (16), the q-axis current relation is

$$i_{sq3} = \frac{k_3}{3}\frac{L_{r3}\psi_{m3}}{L_{m3}L_{\sigma r3}}\sin(3\sin^{-1}(\frac{L_{m1}L_{\sigma r1} i_{sq1}}{L_{r1}\psi_{m1}})) \tag{20}$$

Then, the direct current for third harmonic plane can be derived by vectors relation

$$i_{sd3} = \frac{\psi_{m3}}{L_{m3}}\cos(3\sin^{-1}(\frac{L_{m1}L_{\sigma r1} i_{sq1}}{L_{r1}\psi_{m1}})) \tag{21}$$

The direct and quadrature current derivation in (20) and (21) can meet the air-gap flux density distribution, but the method can't satisfy the slip frequency equation in (5). There is a contradiction for meeting Eqs. (5), (15) and (17) simultaneously. The direct and quadrature current variation in the third harmonic plane can satisfy only two equations.

Hence, another control freedom should be added. In fact, the rotor flux orientations are not required to set at the same direction. Furthermore, the specific flux orientation variation can be used for another control freedom, and the contradiction mentioned above can be solved.

The third harmonic rotor flux orientation can be utilized for another control degree, and the angle relationship in Eq.

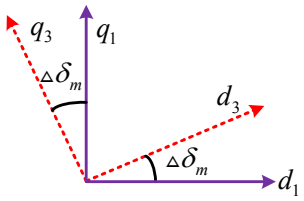

Fig. 5. Rotor flux orientation for fundamental and third harmonic plane

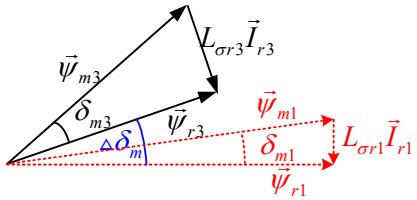

Fig. 6. Air-gap flux distribution with different rotor flux orientation

(15) is also changed. The differential angle $\triangle\delta_m$ between two fluxes is shown in Fig. 5.

Assuming the proportional gain between direct and quadrature

$$k_p = i_{sq1} / i_{sd1} \tag{22}$$

Substituting (22) into slip frequency Eq (5), the quadrature in the third harmonic plane is

$$i_{sq3} = \frac{3\tau_3}{\tau_1} k_p i_{sd3} \tag{23}$$

Substituting (19) and (22) into (17) and (18), the direct current in the third harmonic plane is derived

$$i_{sd3} = \frac{11\sqrt{1+\left(L_{\sigma r1}k_p / L_{r1}\right)^2}}{18\sqrt{1+\left(3L_{\sigma r3}k_p\tau_3 / (\tau_1 L_{r3})\right)^2}} i_{sd1} \tag{24}$$

The quadrature current in the third harmonic plane is

$$i_{sq3} = k_p \frac{33\tau_3\sqrt{1+\left(L_{\sigma r1}k_p / L_{r1}\right)^2}}{18\tau_1\sqrt{1+\left(3L_{\sigma r3}k_p\tau_3 / (\tau_1 L_{r3})\right)^2}} i_{sd1} \tag{25}$$

Hence, the direct and quadrature currents in (20) and (21) are corrected for (24) and (25). The δ_{m1} and δ_{m3} can be derived by as follow

$$\begin{cases} \delta_{m1} = arc\tan\dfrac{L_{\sigma r1} i_{sq1}}{L_{r1} i_{sd1}} \\ \delta_{m3} = arc\tan\dfrac{L_{\sigma r3} i_{sq3}}{L_{r3} i_{sd3}} \end{cases} \tag{26}$$

From expression (24), the phase angle relation in (15) is satisfied when the load is set to zero. However, the third harmonic rotor flux orientation should be real-time adjusted when the mechanical is changed.

The expression for $\triangle\delta_m$ is

$$\triangle\delta_m = 3\delta_{m1} - \delta_{m3} \tag{27}$$

$$\boldsymbol{T}_s = \frac{2}{5}\begin{bmatrix} 1 & \cos(\alpha) & \cos(2\alpha) & \cos(3\alpha) & \cos(4\alpha) \\ 0 & \sin(\alpha) & \sin(2\alpha) & \sin(3\alpha) & \sin(4\alpha) \\ \cos(\triangle\delta_m) & \cos(3\alpha+\triangle\delta_m) & \cos(6\alpha+\triangle\delta_m) & \cos(9\alpha+\triangle\delta_m) & \cos(12\alpha+\triangle\delta_m) \\ \sin(\triangle\delta_m) & \sin(3\alpha+\triangle\delta_m) & \sin(6\alpha+\triangle\delta_m) & \sin(9\alpha+\triangle\delta_m) & \sin(12\alpha+\triangle\delta_m) \\ 1/2 & 1/2 & 1/2 & 1/2 & 1/2 \end{bmatrix}$$

$$\alpha = 2\pi / 5 \tag{28}$$

Accordingly, the orthogonal matrix is modified for Eq (28), which has differential angle in third harmonic plane. The vectors relation between fundamental and third harmonic plane is shown in Fig. 6. The third harmonic flux orientation is changed in time due to load variation, which is not synchronized with fundamental flux orientation.

4. Simulation Results with Proposed Method

A control scheme obtained in Section III has been developed, and its block diagram is shown in Fig. 7, which can be ideally divided into two components with different aims. The first components concerns the current control loop, the second one is the tracking of speed reference. In Fig. 7, the controlled variables are expressed in two reference frames d_1–q_1 and d_3–q_3, which are synchronized and aligned with the corresponding rotor flux orientations.

The proposed method is test for no-load and rated load, and the speed reference is set at 600 r/min. The motor is mechanically load with a step torque of rated value at 2.0 s. The direct and quadrature current components for both planes are shown in Fig. 8. Fig. 8(c) and Fig. 8(d) show

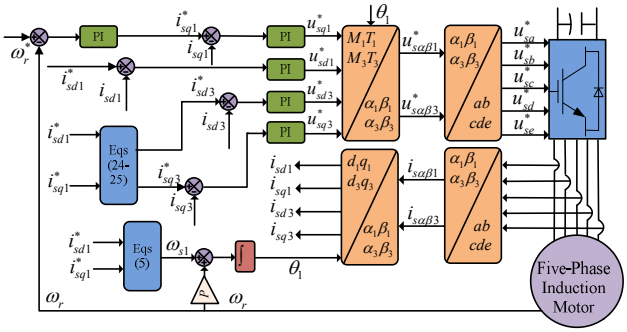

Fig. 7. Block diagram of vector control for five-phase induction motor with third harmonic rotor flux orientation adjustment

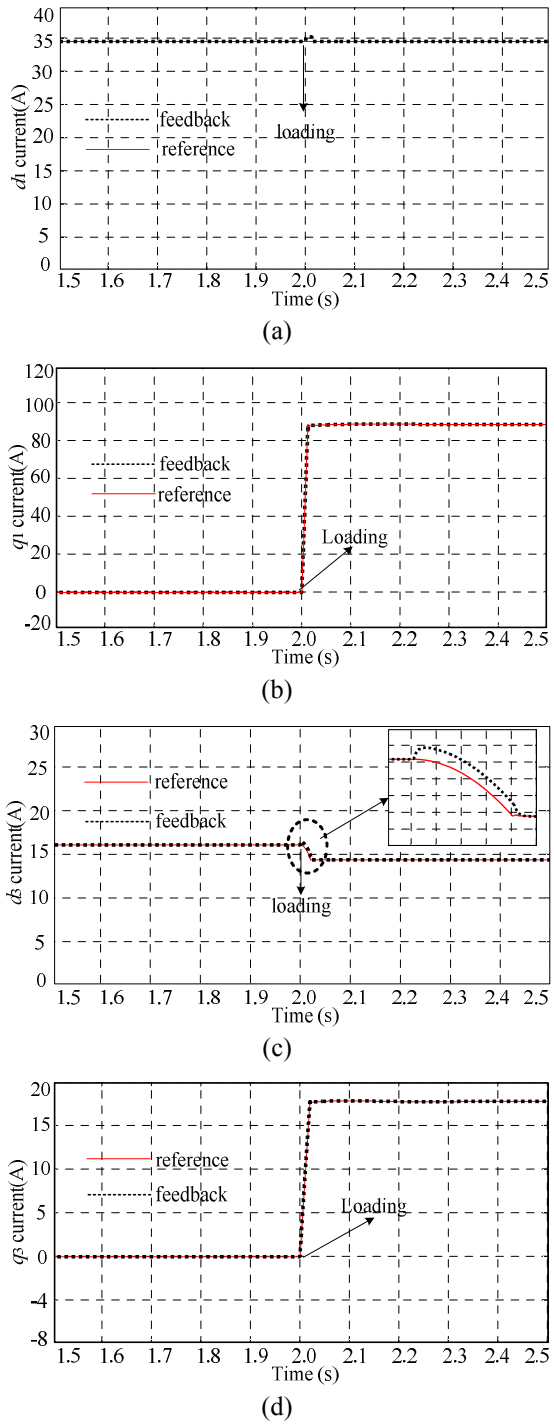

Fig. 8. Simulation results for the proposal method under loading operation: (a) $d1$ current; (b) $q1$ current; (c) $d3$ current; (d) $q3$ current

the variation of the direct and quadrature currents for the proposed method. The quadrature current is linearly proportional to the mechanical loading, while the direct current i_{sd3} decreases with mechanical loading. The ratio between the current components (i_{sd1}, i_{sd3}) and (i_{sq1}, i_{sq3}) are not constant compared with the traditional method.

Fig. 9 demonstrates the EMF distribution simulation

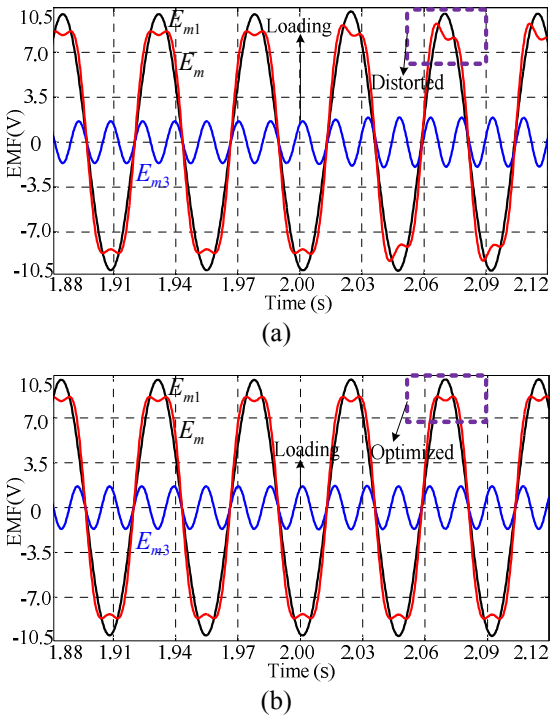

Fig. 9. Simulation results for EMF distribution under loading operation: (a) the conventional method; (b) the proposal method

results for the conventional and proposed methods. The air-gap flux distribution with the conventional method is distorted after mechanical loading. One peak increases and the other decreases compared with no-load case. However, the flux distribution with the proposed method is approximately the same as no-load case, and the amplitude is increased slightly. The proposed method validates the control objective, and air-gap flux density distribution isn't affected by mechanical loading.

5. Experimental Results and Discussion

5.1 System implementation

The basic configuration of experimental system is presented in Fig. 10. It consists of five-phase IM interfaced with a digital control board based on a TMS320F28335. Coupled with a Vortex loader, multiphase motor is driven by a five-phase voltage-source inverter, which operates at 10 kHz switching frequency. The air-gap flux distribution can be obtained by measuring the EMF with search coil within one stator phase, which is occupied in the same slots.

5.2 Air-gap flux distribution with conventional method

The conventional method experimental results for dual-

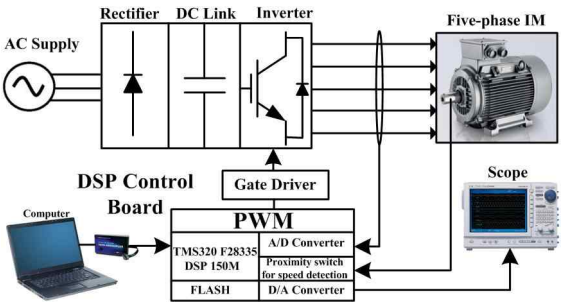

Fig. 10. The platform for the motor testing

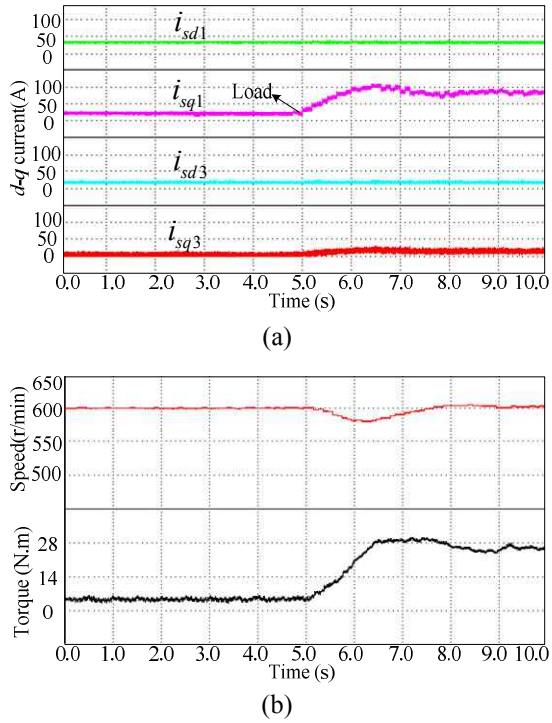

Fig. 11. Experimental results of load operation for conventional method: (a) stator current locus on the *d-q* frame; (b) speed and torque

plane vector control under mechanical load variation are shown in Fig. 11. The speed command is 600 r/min, and speed and torque values are measured by JN 380 transducer. The quadrature currents i_{sq1} and i_{sq3} are approximately proportional to mechanical load, while the direct currents i_{sd1} and i_{sd3} are constant. It should be noted that there is no-load torque with Vortex loader rotation, and the value is about 5.0 N.m at 600r/min.

Fig. 12 demonstrates the conventional method results of stator current and EMF, and the Vortex loader is removed. The stator current is magnetized component without any torque component, and the EMF distribution is presented in Fig. 12(b). The desired air-gap flux density distribution is achieved without load for the conventional method.

Fig. 13 shows the experimental results for the conventional method under rated load condition. The EMF waveform in Fig.13(b) has an obvious distortion, and the

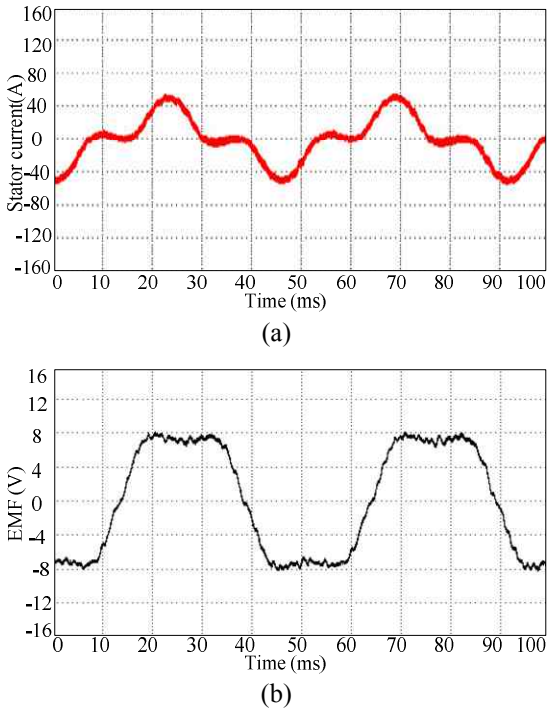

Fig. 12. Experimental results for the conventional method under no-load: (a) stator current; (b) EMF distribution

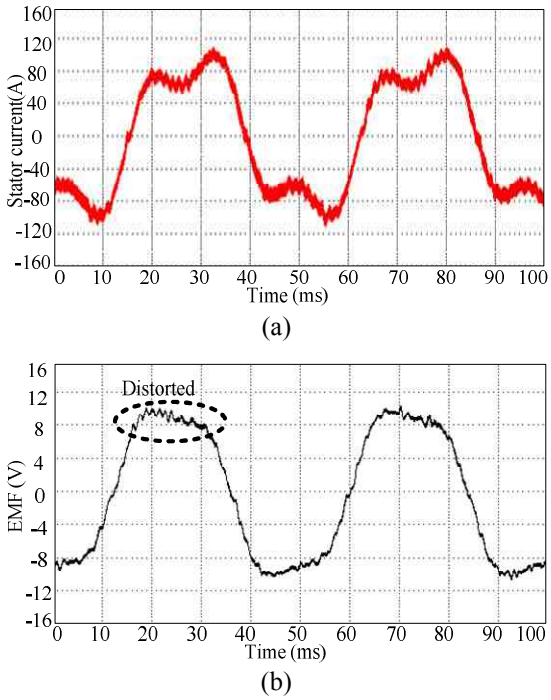

Fig. 13. Experimental results for the conventional method under rated load: (a) stator current; (b) EMF distribution

distortion degree is determined by mechanical load. The first peak is enlarged, and the second peak is minimized. The amplitude distortion degree is about 25.2%.

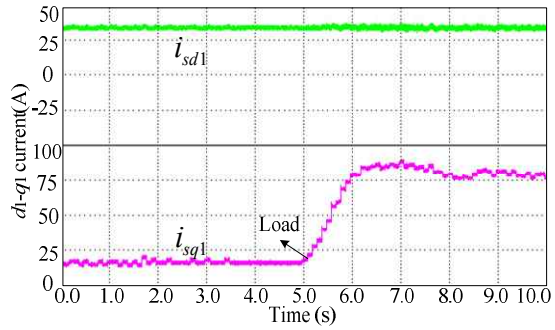

(a)

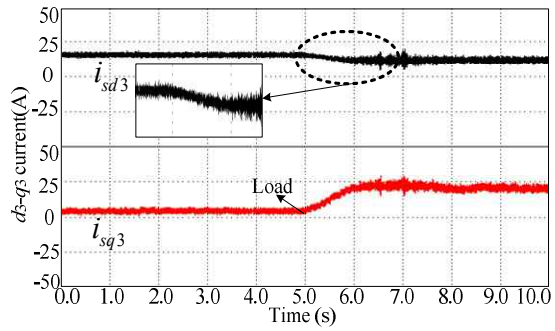

(b)

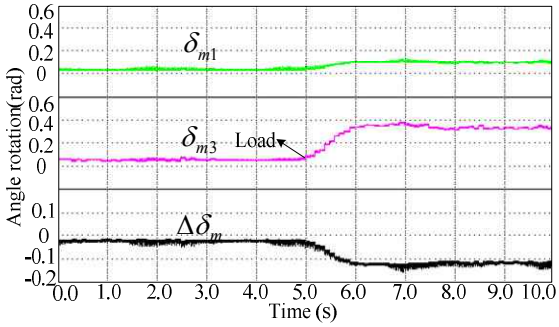

(c)

Fig. 14. Experimental results of d-q current for the proposed method: (a) d_1-q_1 current; (b) d_3-q_3 current; (c) rotor flux angle

5.3 Air-gap flux distribution with proposed method

Fig. 14 demonstrates the performance of the direct and quadrature currents for the proposed method. The direct current i_{sd1} is constant, and the quadrature current is proportional to loading variation. However, the direct and quadrature current for the third harmonic plane as nonlinear function relation, and it depends on mechanical loading. The direct current is decreased by 28.1% at rated load, and the quadrature current is increased by 52.4% compared with conventional method. The rotor flux orientation angle is depicted in Fig. 14(c), and δ_{m1} is not three times as large as δ_{m3}. The differential angle $\Delta\delta_m$ has nonlinear function relationship with mechanical loading, and angle value becomes larger from no-load to rated-load conditions.

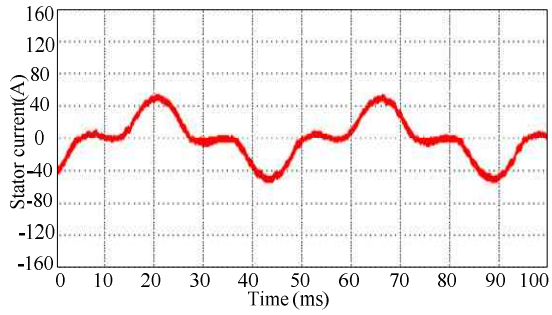

(a)

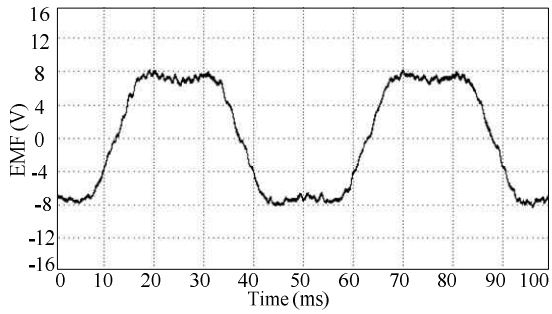

(b)

Fig. 15. Experimental results for the proposed method under no-load: (a) stator current; (b) EMF distribution.

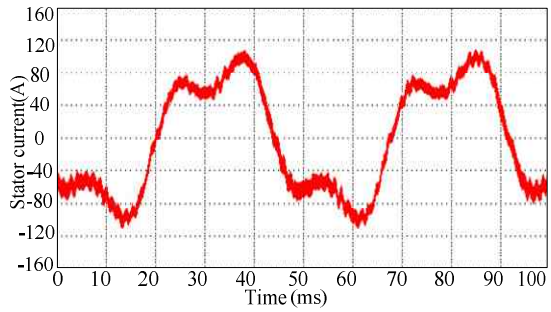

(a)

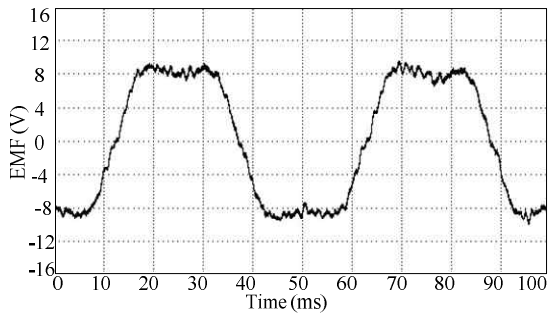

(b)

Fig. 16. Experimental results for the proposed method under rated load: (a) stator current; (b) EMF distribution

Fig. 15 shows the experimental results for the proposed method with no-load, and waveforms are identical with ones in Fig. 12. The air-gap flux density is affected by the leakage rotor flux in the *q*-axis, and the quadrature current is zero without mechanical loading. Hence, the air-gap flux density distribution are the same for both methods.

The air-gap flux density distribution with proposed method is depicted in Fig. 16, when the mechanical load is increased to rated value. The air-gap flux density distribution is optimized, while the result in Fig. 13 is distorted with the conventional method. For the proposed method, the desired air-gap flux density distribution can be obtained under various mechanical loading conditions, and the amplitude of flux density increases with loading increment. The EMF value is increased by 18.5% compared with performance under no-load condition. The reason is that the direct air-gap flux maintain constantly in the IFOC, and the quadrature one increases with load increment.

6. Conclusion

This paper investigates optimum air-gap flux distribution with third harmonic rotor flux orientation adjustment for five-phase induction motor. The proposed method is compared with the conventional method, which has constant current gains between the fundamental and third harmonic planes. The proposed method is designed to achieve the desired air-gap flux density distribution with various mechanical loading, which overcomes the flux distortion problem in the conventional method. The nonlinear current functions between fundamental and third harmonic planes are derived, and the third harmonic flux orientation is real-time adjusted with loading variation. It is confirmed that the proposed method guarantees complete both planes decoupling, since the third harmonic rotor flux orientation is utilized as another control freedom. Nearly rectangular air-gap flux is obtained with the proposed method, and iron utilization is improved. The proposed method is validated by transient and steady-state experimentation.

Acknowledgements

This work was supported by the National Natural Science Foundation of China under Project 51607078, 51407161. It was also supported by National Key Research and Development Plan under Grant 2017YFB0102301.

Appendix

The main dimensions and rated parameters for five-phase IM are demonstrated in Table 1 and Table 2, respectively.

Table 1. Main dimensions of five-phase IM

-	Value	Parameter	Value
Outer diameter (mm)	165	Teeth width(mm)	4.28
Inner diameter (mm)	104	Stator slots	40
Air-gap length (mm)	0.4	Rotor slots	26
Yoke length (mm)	14	Connection	star

Table 2. Parameters of five-phase IM

Parameter	Value	Parameter	Value
Rated Power (kW)	5.0	Rated torque (N.m)	25.0
Rated voltage (V)	19.0	Rs (mΩ)	11.0
Rated current (A)	73.0	R_{r1} (mΩ)	8.1
Number of poles	2	R_{r3} (mΩ)	7.8
Rated speed (rpm)	1940	L_{m1} (mH)	1.63
Rated frequency (Hz)	66.7	L_{m3} (mH)	0.15

References

[1] E. Levi, "Multiphase electric machines for variable-speed application," *IEEE Trans. Ind. Electron.*, vol. 55, no. 5, pp. 1893-1909, May 2008.

[2] E. Levi, R. Bojoi, F. Profumo, H. A. Toliyat, and S. Williamson, "Multiphase IM drives – A technology status review," *IET Elect. Power Appl.*, vol. 1, no. 4, pp. 489-516, Jul. 2007.

[3] R. Bojoi, F. Profumo, and A. Tenconi, "Dual-three phase IM drives-a technology status review," *IET Electr. Power Appl.*, vol. 126, no. 4, pp. 420-429, 2006.

[4] H. A. Toliyat, L. Y. Xu, and T. A. Lipo, "A five-phase reluctance motor with high specific torque," *IEEE Trans. Ind. Appl.*, vol. 28, no. 3, pp. 659-667, May/ Jun. 1992.

[5] H. A. Toliyat, T. A. Lipo, and J. White, "Analysis of a concentrated winding induction machine for adjustable speed drive applications. II. Motor design and performance," *IEEE Trans. Energy Convers.*, vol. 6, no. 4, pp. 684-692, Dec. 1991.

[6] D. Suman and L. Parse, "Fault-tolerant control of five-phase permanent-magnet motors with trapezoidal back EMF," *IEEE Trans. Ind. Electron.*, vol. 58, no.2, pp. 476-485, Feb. 2011.

[7] A. Mohammadpour, S. Sadeghi, and L. Parsa, "A generalized fault-tolerant control strategy for five-phase PM motor drives considering star, pentagon, pentacle connections of stator windings," *IEEE Trans. Ind. Electron.*, vol. 61, no. 1, pp. 63-75, Jan. 2014.

[8] H. Guzman, M. J. Duran, F. Barrero, B. Bogado, and S. Toral, "Speed control of five-phase IMs with integrated open-phase fault operation using model-based predictive current control techniques," *IEEE Trans. Ind. Electron.,* vol. 61, no. 9, pp. 4474-4484, Aug.2013.

[9] H. Guzman, F. Barrero, and M. J. Duran, "IGBT-gating failure effect on a fault-tolerant predictive current-controlled five-phase induction motor drive," *IEEE Trans. Ind. Electron.*, vol. 62, no. 1, pp. 15-20,

Jan. 2015.
[10] A. Mohammadpour and L. Parse, "Global fault-tolerant control technique for multiphase permanent-magnet machines," *IEEE Trans. Ind. Electron.*, vol. 51, no. 1, pp. 178-186, Jan./ Feb. 2015.
[11] H. S. Che, E. Levi, M. Jones, W. Hew, and N. Abd. Rahim, "Current control methods for an asymmetrical six-phase IM drive," *IEEE Trans. Ind. Electron.*, vol. 29, no. 1, pp. 407-417, Jan.2014.
[12] A. G. Yepes, J. Malvar, A. Vidal, O. López, and J. Doval-Gandoy, "Current harmonics compensation based on multiresonant control in synchronous frames for symmetrical *n*-phase machines," *IEEE Trans. Ind. Electron.*, vol. 62, no. 5, pp. 2708-2720, May. 2015.
[13] L. Parsa, and H. A. Toliyat, "Five-phase permanent-magnet motor drives," *IEEE Trans. Ind. Appl.*, vol. 41, no. 1, pp. 30-37, Jan./Feb. 2005.
[14] H. Xu, H. A. Toliyat, and L. J. Petersen, "Five-phase IM drives with DSP-based control system," *IEEE Trans. Power Electron.*, vol. 17, no. 4, pp. 524-533, Jul. 2002.
[15] O. Dordevic, M. Jones, and E. Levi "Analytical formulas for phase voltage RMS square and THD in PWM multiphase system," *IEEE Trans. Ind. Electron.*, vol. 30, no. 8, pp. 1645-1656, March. 2015.
[16] N. Bode, M. Jones, and E. Levi, "A space vector PWM with common-mode voltage elimination for open-end winding five-phase drives with a single DC supply," *IEEE Trans. Ind. Electron.*, vol. 61, no. 5, pp. 2197-2207, May. 2014.
[17] N. Bodo, E. Levi, and M. Jones, "Investigation of carrier-based PWM techniques for a five-phase open-end winding drive topology," *IEEE Trans. Ind. Electron.*, vol. 60, no. 5, pp. 2054-2065, May. 2013.
[18] G. Carrasco and C. A. Silva, "Space vector PWM method for five-phase two-level VSI with minimum harmonic injection in the over-modulation region," *IEEE Trans. Ind. Electron.*, vol. 60, no. 5, pp. 2042-2205, May. 2013.
[19] J. Wang, R. Qu, and L. Zhou, "Dual-rotor multiphase permanent magnet machine with harmonic injection to enhance torque density," *IEEE Trans. Appl. Supercond.*, vol. 22, no. 3, pp. 5202204, Jun. 2012.
[20] H. Xu, H. A.Toliyat, and L. J. Petersen, "Rotor field oriented control of five-phase IM with the combined fundamental and third harmonic currents," in *Proc. IEEE APEC*, Anaheim, CA, 2001, pp. 392-398.
[21] M. J. Duran, F. Salas, and M. R. Arahal, "Bifurcation analysis of five-phase IM drives with third harmonic injection," *IEEE Trans. Ind. Electron.*, vol. 55, no. 5, pp. 2006-2014, May. 2008.
[22] C. C. Scharlau, L. F. A. Pereira, L. A. Pereira, and S. Haffner, "Performance of a five-phase induction machine with optimized air gap field under open loop V/f control," *IEEE Trans. Energy Convers.*, vol. 23, no. 4, pp. 1046-1056, Dec. 2008.
[23] L. A. Pereira, C. C. Scharlau, L. F. Pereira, and J. F. Haffner, "General model of a five-phase induction machine allowing for harmonics in the air gap field," *IEEE Trans. Energy Convers.*, vol. 21, no. 4, pp. 891-899, Dec. 2006.
[24] R. O. C. Lyra, and T. A. Lipo, "Torque density improvement in a six-phase IM with third harmonic current injection," *IEEE Trans. Ind. Appl.*, vol. 38, no. 5, pp. 1351-1360, Sep./ Oct. 2002.
[25] A. Yong-Le, M. J. Kamper, and A. D. Roux, "Novel direct flux and direct torque control of six-phase induction machine with nearly square air-gap flux density," *IEEE Trans. Ind. Appl.*, vol. 43, no. 6, pp. 1534-1543, Nov./ Dec. 2007.
[26] A. Abdel-Khalik, M. Masoud, and W. Barry, "Eleven-phase induction machine: Steady-state analysis and performance evaluation with harmonic injection," *IET Elect. Power Appl.*, vol. 4, no. 8, pp. 670-685, Sep. 2010.
[27] A. S. Abdel-Khalik, M. I. Masoud, and B. W. Williams, "Optimum flux distribution with harmonic injection for a multiphase induction machine using genetic algorithms," *IEEE Trans. Energy Convers.*, vol. 26, no. 2, pp. 501-512, Jun. 2011.
[28] A. S. Abdel-Khalik, M. I. Masoud, S. Ahmed, and A. M. Massoud, "Effect of current harmonic injection on constant rotor volume multiphase induction machine stators: A comparative study," *IEEE Trans. Ind. Appl.*, vol. 48, no. 6, pp. 2002-2013, Nov./Dec. 2012.
[29] M. Mengoni, L. Zarri, A. Tani, L. Parsa, G. Serra, and D. Casadei, "High-torque-density control of multiphase induction motor drives operating over a wide speed range," IEEE Trans. Ind. Electron., vol. 62, no. 2, pp. 814-825, Feb. 2015.
[30] L. Zheng, J. E. Fletcher, B. W. Williams, and X. He, "Dual-plane vector control of a five-phase induction machine for an improved flux pattern," IEEE Trans. Ind. Electron., vol. 55, no. 5, pp.1996-2005, May. 2008.
[31] A. S. Abdel-Khalik, M. I. Masoud, and B. W. Williams, "Improved flux pattern with harmonic injection for multiphase induction machines," IEEE Trans. Ind. Electron., vol. 27, no. 3, pp. 1563-1578, Mar. 2012.

Min Kang received the B.S. and Ph.D. degrees from the College of Electrical Engineering, Zhejiang University, Hangzhou, China, in 2003 and 2008, respectively. From 2008 to 2011, he was a Lecturer in the College of Electrical Engineering, Zhejiang University of Science and Technology, China. He is currently associate Professor of Zhejiang of Science and Technology. His research interests are in multiphase bearingless machines and AC drives.

Wenjuan Yu was born in shandong, China, in 1986. She received the B.S. degree from Huazhong University of Science &Technology, Wuhan, in 2008. She received the M.S. degree from Zhejiang University, Hangzhou, in 2011. Her research interests are high-power multiphase motor drives.

Zhengyu Wang was born in Hunan, China, in 1980. He received the Bachelor of Engineering degree from Xian Jiaotong University in 2002, and the Master of Engineering degree from Southwest Jiaotong University in 2014, respectively. He had been working at CRRC Zhuzhou Institute and engaged in the field of electric machine control design from Aug 2002 to Jan 2007,after that he has been working at Hunan CRRC Times Electric Vehicle and engaged in the field of motor drive control system design until now.

Wubin Kong (M'15) was born in Zhejiang, China, in 1986. He received the B.S. and Ph.D. degree from Zhejiang University, Hangzhou, China in 2009 and 2014, respectively. His research interests are high-power multiphase motor drives and fault tolerant control motor drive applied in EV. From 2015, he has been a lecture with Huazhong University of Science &Technology, Wuhan, China.

Ye Xiao was born in Hunan, China, in 1981. He received a bachelor's degree from Beijing University of nation-nalities, Beijing, China in 2005. His main research direction is the motor control of new energy vehicles.